nature neuroscience

# Parcellating cortical functional networks in individuals

Danhong Wang[1,2], Randy L Buckner[1–3], Michael D Fox[1,4,5], Daphne J Holt[1,2], Avram J Holmes[2,6], Sophia Stoecklein[1,7], Georg Langs[8,9], Ruiqi Pan[1], Tianyi Qian[1,10,11], Kuncheng Li[12], Justin T Baker[2,13], Steven M Stufflebeam[1,14], Kai Wang[15], Xiaomin Wang[16], Bo Hong[10] & Hesheng Liu[1,2]

**The capacity to identify the unique functional architecture of an individual's brain is a crucial step toward personalized medicine and understanding the neural basis of variation in human cognition and behavior. Here we developed a cortical parcellation approach to accurately map functional organization at the individual level using resting-state functional magnetic resonance imaging (fMRI). A population-based functional atlas and a map of inter-individual variability were employed to guide the iterative search for functional networks in individual subjects. Functional networks mapped by this approach were highly reproducible within subjects and effectively captured the variability across subjects, including individual differences in brain lateralization. The algorithm performed well across different subject populations and data types, including task fMRI data. The approach was then validated by invasive cortical stimulation mapping in surgical patients, suggesting potential for use in clinical applications.**



The human cerebral cortex is organized into areas on the basis of distinct features such as cytoarchitecture and topography[1–5]. These brain areas contribute specialized functions that interact as part of distributed networks[1,6,7]. Recent advances in noninvasive neuroimaging techniques, especially the emergence of functional connectivity MRI[8,9], have made it possible to explore the functional organization of regions and networks in the living human brain[10–15]. Initial work has revealed a number of complexities including aspects of organization that respect traditional notions of brain areas, as well as network organization that has organizational properties that span and split areas. Furthermore, there are individual differences in organization that are distributed nonuniformly across the cortex. Obtaining functional atlases at the level of the individual is a critical step toward understanding the association between anatomy and function in the human brain and the stability of this relationship across individuals[16].

The capacity to identify the unique functional architecture of an individual's brain is particularly important for personalized medicine. Clinical and imaging studies, including those employing invasive functional mapping techniques, have demonstrated marked inter-individual variability in the organization of different functional systems of the brain[17–19]. Localizing functional architecture in a particular subject is therefore a fundamental requirement in clinical procedures such as surgical planning[20] and brain stimulation therapies[21,22]. However, noninvasive functional mapping techniques are generally limited in accuracy and reliability at the single-subject level[23]. To date, precise functional mapping in individual patients still relies heavily on invasive measures.

Individual-level functional mapping is also essential for the investigation of variations in human behavior and cognition. Functional imaging studies of individual differences commonly use regions of interest (ROIs) defined by anatomy or by population-averaged fMRI studies[24]. To improve specificity, individual-level ROIs can be defined using a task-based functional localizer[25]. Recently, increased effort has been devoted to developing methods for parcellating functional networks in individual subjects on the basis of resting-state connectivity[14,16,26–30]. An individual-level functional parcellation can not only be used as the 'localizer' for specific functions, but can also provide a basis for cross-subject alignment according to functional characteristics, instead of macroscopic anatomical landmarks, to improve group-level analyses.

Achieving individual-level precision is thus a major goal of neuroimaging. Specifically, to be clinically useful, a noninvasive functional mapping technology must fulfill the following criteria: (i) it should have high reproducibility within subjects, (ii) it should be sensitive to functional differences between subjects and (iii) it should match results derived from invasive cortical stimulation, currently considered the gold standard for individual-level functional mapping. On the basis of these criteria, we have developed an

[1]Athinoula A. Martinos Center for Biomedical Imaging, Department of Radiology, Massachusetts General Hospital, Harvard Medical School, Charlestown, Massachusetts, USA. [2]Department of Psychiatry, Massachusetts General Hospital, Harvard Medical School, Boston, Massachusetts, USA. [3]Department of Psychology, Center for Brain Science, Harvard University, Cambridge, Massachusetts, USA. [4]Berenson-Allen Center for Noninvasive Brain Stimulation, Department of Neurology, Beth Israel Deaconess Medical Center, Harvard Medical School, Boston, Massachusetts, USA. [5]Department of Neurology, Massachusetts General Hospital, Harvard Medical School, Boston, Massachusetts, USA. [6]Department of Psychology, Yale University, New Haven, Connecticut, USA. [7]Ludwig Maximilians University Munich, Institute of Clinical Radiology, Munich, Germany. [8]Computational Imaging Research Lab, Department of Biomedical Imaging and Image-guided Therapy, Medical University of Vienna, Vienna, Austria. [9]Computer Science and Artificial Intelligence Lab, Massachusetts Institute of Technology, Cambridge, Massachusetts, USA. [10]Department of Biomedical Engineering, School of Medicine, Tsinghua University, Beijing, China. [11]Siemens Healthcare, MR Collaboration Nebraska Asia, Beijing, China. [12]Department of Radiology, Xuanwu Hospital, Capital Medical University, Beijing, China. [13]Psychotic Disorders Division, McLean Hospital, Belmont, Massachusetts, USA. [14]Harvard-MIT Health Sciences and Technology, Institute for Medical Engineering and Science, Cambridge, Massachusetts, USA. [15]Department of Neurology, the First Affiliated Hospital of Anhui Medical University, Hefei, China. [16]Beijing Institute for Brain Disorders, Capital Medical University, Beijing, China. Correspondence should be addressed to H.L. (hesheng@nmr.mgh.harvard.edu) or B.H. (hongbo@tsinghua.edu.cn).

Received 16 September; accepted 14 October; published online 9 November 2015; doi:10.1038/nn.4164

approach for individual-level functional parcellation based on functional connectivity, which can be applied to resting-state fMRI data or spontaneous activity extracted from task fMRI data. Test-retest reliability of the parcellation and its sensitivity to individual differences were evaluated on multiple data sets. Validity of the network parcellation was then examined in a group of surgical patients who underwent invasive cortical stimulation.

The parcellation strategy was as follows:

1. A functional cortical atlas consisting of 18 networks was first estimated on the basis of data from 1,000 healthy subjects[10] and projected onto the individual subject's cortical surface using the FreeSurfer software (Online Methods). The individual subject's blood oxygenation level–dependent (BOLD) fMRI signal time courses were then averaged across the vertices that fell within each network. These atlas-based network time courses were used as the 'reference signals' for the subsequent optimization procedure.

2. The individual subject's functional MRI signal at each vertex was then correlated to the 18 reference signals derived from the previous step. Each vertex was reassigned to one of the 18 networks according to its maximal correlation to the reference signals. A confidence value was also computed as the ratio between the largest and the second-largest correlation values. For example, if a vertex had the strongest correlation with the reference signal of network A, with a correlation coefficient of 0.8, and the second-strongest correlation with the network B, with a correlation coefficient of 0.4, the confidence that this vertex belongs to network A was 0.8/0.4 = 2. After all vertices were reassigned to one of the 18 networks with a certain confidence level, in each network the BOLD signals of vertices with a confidence value greater than a preselected threshold (for example, >1.1) were averaged and termed the 'core signal'. Several parameters were computed for each network, including the pre-estimated inter-subject variability in functional connectivity[31] and temporal signal-to-noise ratio (SNR), which were normalized and averaged across the vertices where the confidence values exceeded the given threshold.

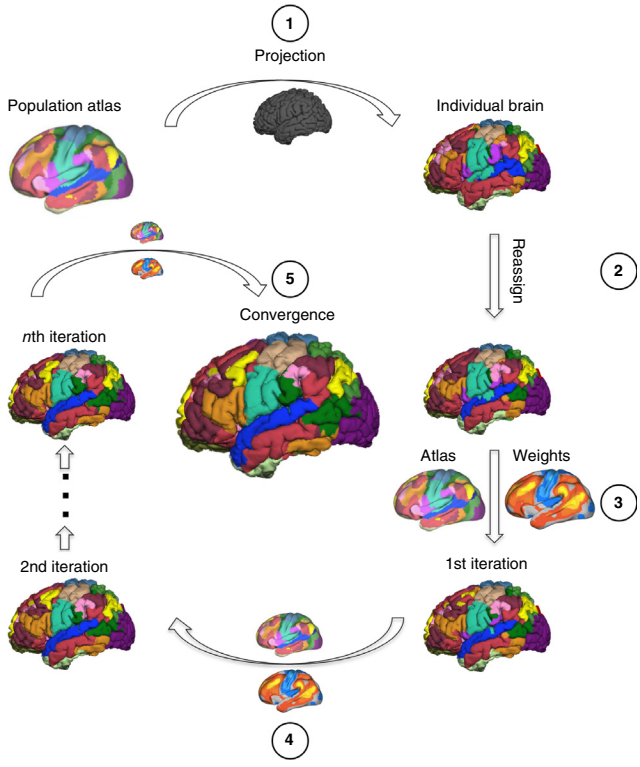


3. For each network, the core signal derived from step (2) and the original reference signals derived from step (1) were averaged in a weighted manner. Before averaging, the core signal was multiplied by the weighting parameters computed in step (2), including inter-subject variability, SNR and number of iterations. The resulting signal estimate was used as the new reference signal for the next iteration. This weighting strategy ensured that the original atlas-based reference signal was weighted less than the core signal in regions of high inter-subject variability and regions of high SNR. The weights were gradually reduced as the iteration proceeded. Using these new reference signals, which incorporated both the individual subject's information and the information of the population atlas, the brain vertices were further reassigned to one of the 18 networks.

4. Steps (2) and (3) were iterated until the algorithm reached a predefined stopping criterion; for example, the procedure was stopped if network membership remained the same for 98% of the vertices in two consecutive iterations or after a predetermined number of iterations.

## RESULTS

### Maps are reliable and capture inter-subject variability

We first applied the parcellation technique (**Fig. 1**) to a longitudinal data set (data set I) consisting of 23 subjects who were scanned five times within a period of six months. During the iterative search, the boundaries of the functional networks were gradually refined according to the connectivity patterns estimated in individual data but guided by the population-atlas (**Supplementary Fig. 1** shows an example of the intermediate results after each iteration). In general, vertices in the primary visual and sensorimotor regions showed relatively stable network membership assignment over the iterations. However, vertices in the association cortices showed greater adjustment during the optimization process.

Within each subject, the resulting functional atlases converged to be visually consistent across the five sessions, both in the primary sensorimotor regions and the higher-order association regions (**Fig. 2**). Quantitative analyses indicated high intra-subject reproducibility across the five sessions (mean Dice coefficient = 83%). At the same time, functional maps varied substantially across different individuals (mean Dice coefficient = 67%), especially in the higher-order association regions. These results indicate that the iterative parcellation

**Figure 1** Parcellating the functional networks in an individual subject's brain using an iterative adjusting approach. The technique includes the following steps: (1) A population-based functional brain atlas is registered onto an individual subject's cortical surface using FreeSurfer. The individual subject's BOLD signal time courses are then averaged across the vertices that fall within each network. These atlas-based network time courses are used as the reference signals for the subsequent optimization procedure. (2) The individual subject's BOLD signal at each vertex is then correlated to the 18 reference signals. Each vertex is reassigned to one of the 18 networks according to its maximal correlation to the reference signals. A confidence value (the ratio between the largest and the second largest correlation values) is computed. After each vertex is reassigned, the BOLD signals of the high confidence vertices (for example, >1.1) in each network are averaged and termed the core signal. (3) For each network, the core signal derived from step (2) and the original reference signals derived from step (1) are averaged in a weighted manner. Specifically, the core signal is multiplied by the weighting parameters derived from inter-subject variability and SNR as well as the number of iterations. The averaged signal is used as the new reference signal for the next iteration. Using these new reference signals, the brain vertices are further reassigned to one of the 18 networks. (4) Steps (2) and (3) are repeated until the algorithm reaches a predefined stopping criterion.

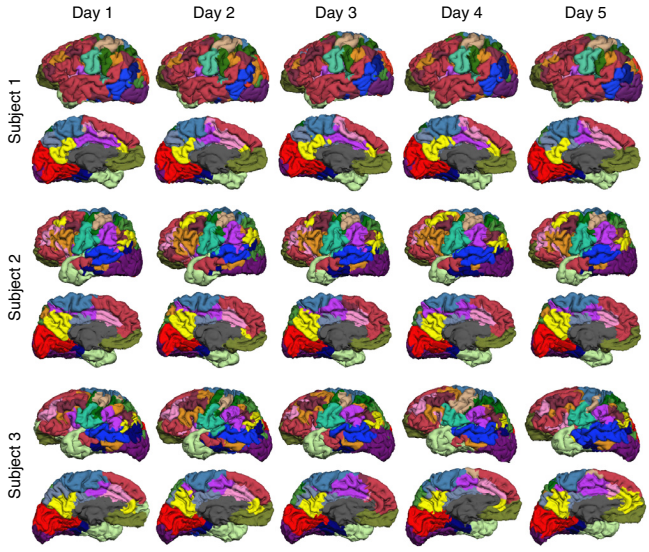


**Figure 2** Iterative brain parcellation is highly reproducible within subjects and captures differences across subjects. Twenty-three healthy subjects underwent five resting-state scanning sessions within 6 months. The functional organization of an individual subject's brain was parcellated into 18 networks using the data of each scanning session. The parcellation networks of three subjects that showed the highest reproducibility across sessions are displayed. The functional maps differed substantially across subjects, especially in the higher-order association areas (**Supplementary Fig. 2** and http://nmr.mgh.harvard.edu/bid/download.html).

technique is able to obtain reliable functional networks for the same person and can reflect the network distribution differences between individuals (**Supplementary Fig. 2** shows maps of three subjects who demonstrated high, median and low reproducibility across sessions). Most notably, each individual brain had unique features.

### Parcellation is widely applicable to different data types

To objectively examine the performance of the iterative parcellation, quantitative analyses of the test-retest reliability and sensitivity to individual differences were performed in a sample independent from data set I that was involved in the algorithm development. MRI data from 100 unrelated volunteers (data set II) publicly available from the Human Connectome Project (HCP) were used for this replication purpose. This cohort was substantially different from data set I in terms of age, scan length, ethnicity, scanner type and scanning protocol. Each volunteer underwent two resting-state fMRI (rs-fMRI) sessions and seven task fMRI sessions (Online Methods). The rs-fMRI sessions were conducted on separate days; thus, they could be used to evaluate the test-retest reliability of the network parcellation.

Intra-subject reliability and inter-subject variability were measured using the Dice coefficient after each iteration (**Fig. 3a**). Because the algorithm was initialized with the population-based atlas, intra-subject reliability was 1 and inter-subject variability was 0 at the beginning. As the iterative procedure progressed, inter-subject variability increased and intra-subject reliability decreased, but both stabilized after several iterations (**Supplementary Fig. 3**).

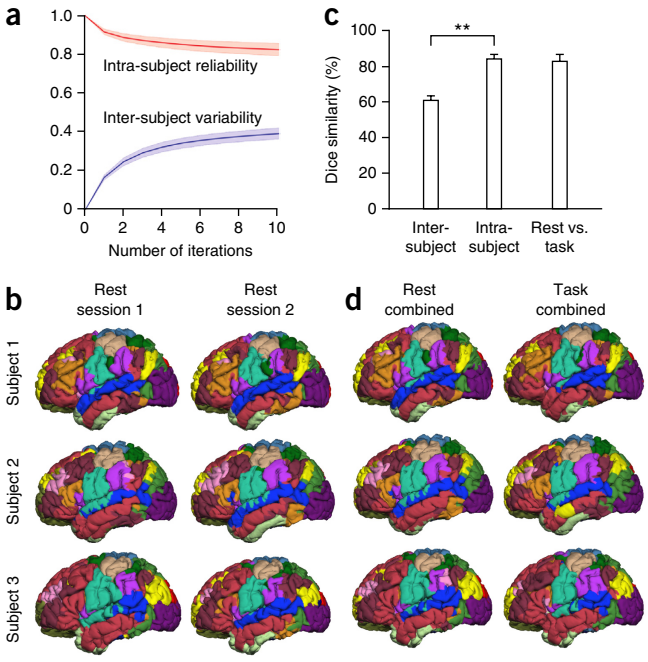


The iterative parcellation technique showed generalizability in this independent data set. Functional maps derived from the two rs-fMRI sessions were highly consistent within subjects (**Fig. 3b** and http://nmr.mgh.harvard.edu/bid/download.html). In comparisons of two rs-fMRI sessions within the same subject, the Dice coefficient was 82.4% ± 3.2% (mean ± s.d.). Notably, the maps also showed substantial inter-subject variability. Between any two individuals, the Dice coefficient was 60.5% ± 2.8% (corresponding to inter-subject variability of 39.5%). The intra-subject consistency of network membership was significantly higher than the inter-subject consistency (unpaired two-tailed *t*-test, $t_{(5048)} = 91.0$, $P < 0.001$) (**Fig. 3c**).

An important question is whether the iterative parcellation technique can be applied to the task fMRI data that are widely available. Given that numerous task fMRI data sets already exist[32] and task fMRI is routinely performed for preoperative mapping in many hospitals, the practical value of this iterative parcellation technique will be greatly enhanced if this technique can be directly applied to task data. To test this possibility, the task-based fMRI data of the 100 HCP subjects were bandpass filtered (0.01–0.08 Hz) and processed in the same way as the resting-state data. Parcellation can be derived from the data of a single task but is less reliable owing to limited data acquisition length (**Supplementary Fig. 4** and Online Methods). The data of different tasks were therefore concatenated within each subject to increase the amount of data per subject and to minimize the impact of any specific task design on the connectivity estimates[33,34]. For each individual subject, iterative parcellation was performed on the concatenated task fMRI data and the concatenated resting-state

**Figure 3** Quantitative analyses of intra-subject reliability and inter-subject variability based on the HCP subjects. (**a**) Intra-subject reliability and variability of the parcellation maps after each iteration. Shaded areas represent s.d. (**Supplementary Fig. 3** shows spatial distributions of reliability and variability after each iteration.) (**b**) Networks of three exemplary subjects. (**c**) Parcellation based on the resting-state fMRI demonstrates high intra-subject reliability and high inter-subject variability. Between any two individuals (inter-subject), only 60.5% ± 2.8% (mean ± s.d.) of the brain vertices were assigned to the same networks. Comparing two sessions for the same subject (intra-subject), 82.4% ± 3.2% (mean ± s.d.) of the vertices were assigned to the same networks. Parcellation results based on task data and resting-state data for all 100 HCP subjects (task vs. rest) showed an overlap of 81.7% ± 4.0% (mean ± s.d.). $^{**}P < 0.001$ (unpaired two-tailed *t*-test). (**d**) Networks derived from the concatenated task data for three exemplary subjects.

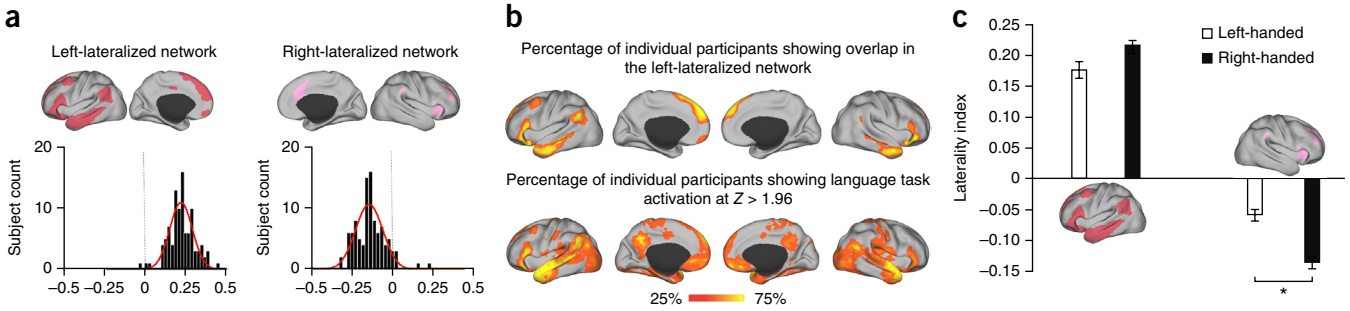


**Figure 4** Brain lateralization is reflected in the network parcellation. (**a**) LIs for the two networks that demonstrated strongest lateralization in the 100 HCP subjects; positive values indicate left lateralization. The strongest left-lateralized network was located in the traditional language area, and the strongest right-lateralized network was located in the traditional ventral attention area. (**b**) The strongest left-lateralized parcellation network overlapped with the regions showing activation during a language task. Maps display the percentage of subjects showing overlap in the left-lateralized network and the percentage of subjects showing language activation ($Z > 1.96$, corresponding to uncorrected, two-tailed $P < 0.05$). Activation maps were estimated using the general linear model. At the group level, 71.2% of the vertices in the left-lateralized network fell within the regions activated by the language task. (**c**) Handedness affects functional network lateralization. The lateralization indices of the language-related and ventral attention-related networks were computed in 52 left-handed and 52 matched right-handed subjects. Right-handed subjects showed stronger lateralization in the language-related network ($P = 0.057$, unpaired two-tailed $t$-test) and significantly stronger lateralization in the ventral attention-related network ($^*P = 0.003$, unpaired two-tailed $t$-test). Error bars, mean ± s.e.m.

data (**Fig. 3d**). Parcellation results based on the task fMRI data and the resting-state data were similar (Dice coefficient = 81.7% ± 4.0%). The consistency between the rest- and task-based parcellation maps was as high as the reproducibility between two resting-state sessions (paired two-tailed $t$-test, $t_{(99)} = 1.76$, $P = 0.08$) (**Fig. 3c**). These results suggest the feasibility of obtaining whole-brain functional atlases of individual subjects from task fMRI data.

### Brain lateralization is reflected in network parcellation

Hemispheric lateralization is an important organizational principle of the human brain and a potential marker of individual differences in brain development[35]. Here we quantified the laterality of network distribution in individual subjects. For each network, a laterality index (LI) was computed on the basis of the number of vertices in the left hemisphere and the number in the right hemisphere (Online Methods). Among the 18 networks that resulted from the iterative parcellation, we identified two that demonstrated strong asymmetry. The most left-lateralized network (LI = 0.22 ± 0.08 (positive LI values indicate left-lateralization)) included the inferior frontal gyrus and the temporal parietal junction—regions traditionally associated with language (**Fig. 4a**). Among the 100 subjects, only a few demonstrated atypical right lateralization of this network (**Fig. 4a**). The most right-lateralized network (LI = −0.13 ± 0.09 (mean ± s.d.)) included the insula and the angular gyrus—traditionally associated with ventral attention[36]. Lateralization of these two networks showed moderate test-retest reliability (**Supplementary Fig. 5**). To directly examine the relationship between the left-lateralized parcellation network and language function, we mapped the regions showing activation (at a $Z$ threshold of $Z > 1.96$, corresponding to uncorrected, two-tailed $P$ threshold of $P < 0.05$) during a story-comprehension task[37]. At the group level, 71.2% of the vertices in the left-lateralized parcellation network fell within the regions showing language-related activation (**Fig. 4b**), suggesting that this left-lateralized network is related to language function.

Finally, we investigated the effect of handedness on functional network laterality in 52 left-handed and 52 right-handed individuals (data set III) matched by age, gender, ethnicity, education, fMRI data acquisition, data quality and other parameters (**Supplementary Table 1**). Iterative parcellation was applied to each individual subject to identify

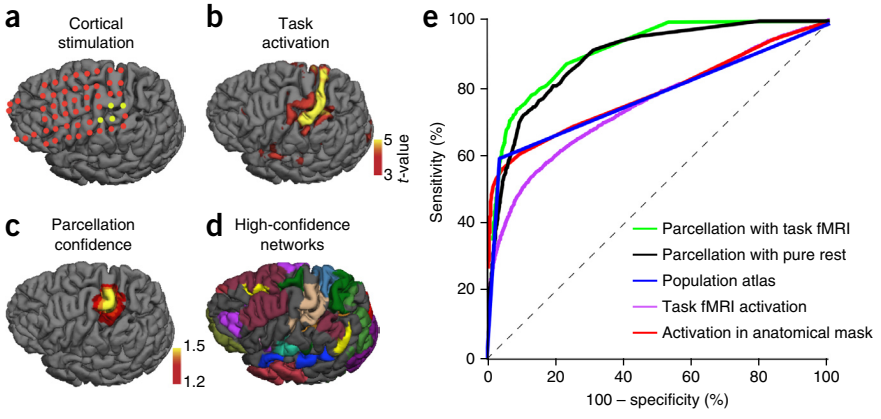


**Figure 5** Sensorimotor networks identified by individual brain parcellation correspond to functional regions localized by invasive cortical stimulation. (**a**) The hand and tongue sensorimotor regions of eight surgical candidates were mapped by multiple approaches. Sensorimotor regions identified by ECS were used as the standard. Red dots indicate negative electrodes; yellow dots indicate positive electrodes. The subject shown here is Patient 2 in **Supplementary Figure 6**. (**b**) Sensory and motor areas identified by traditional task activation show low consistency with the ECS maps. (**c**) The hand sensorimotor regions identified by iterative parcellation based on the concatenated task fMRI data were consistent with the ECS maps. The map shows the vertices with high confidence values (>1.2). (**d**) Individual brain parcellation may serve as a prescreening method for ECS. The map shows the network membership of vertices with high confidence values (>1.1). (**e**) Statistical analysis of sensitivity and specificity of the hand and tongue sensorimotor maps in eight surgical patients across a wide range of thresholds for five mapping approaches: the iterative parcellation technique using task fMRI of eight subjects (green), the iterative parcellation technique using pure resting-state fMRI of six subjects (black), direct projection of the population-based atlas to each individual subject (blue), traditional task-activation mapping alone (purple) and task activation masked with anatomical labels generated by FreeSurfer (red).

the 18 networks. Again, the language-related network and the ventral attention-related network showed the strongest lateralization in both groups. Compared to left-handed subjects, right-handed subjects showed a trend for stronger lateralization in the language-related network (mean LI 0.20 versus 0.16, unpaired two-tailed $t$-test, $t_{(102)} = 1.9$, $P = 0.057$), and significantly stronger lateralization in the ventral attention-related network (mean LI −0.14 versus −0.07, unpaired two-tailed $t$-test, $t_{(102)} = 3.1$, $P = 0.003$) (**Fig. 4c**).

### Comparing parcellation networks with task fMRI

The reliability of task-evoked response in individual subjects is affected by many factors, some of which extend to analysis of resting-state networks and some that are preferential to task fMRI[38]. Many studies have used task fMRI activation maps to validate or evaluate the accuracy of results derived from resting-state fMRI. Here, we quantified the intra-subject reliability of task fMRI activation maps and the functional networks derived from the iterative parcellation. For this investigation, two brain functions that are routinely examined in preoperative mapping, motor and language functions were assessed in data set II (the 100 HCP subjects). The hand motor network and the language network of each subject were localized by conventional task-evoked responses and by iterative network parcellation.

Task-evoked responses were estimated using single task runs and showed a range of intra-subject reliability across two runs. Reliability was evaluated using the Dice coefficient across a variety of thresholds (from $Z = 1.96$ to $Z = 10.0$, in increments of 0.1). The maximum reliability was 40.4% (when $Z = 6.76$) for the motor task and 34.4% (when $Z = 1.96$) for the language task. Iterative parcellation was then performed on short resting-state data segments, with length matched to that of the motor and language task runs (3 m 34 s and 3 m 57 s, respectively). Compared to the task-evoked responses, the iterative parcellation yielded higher reproducibility across two runs (paired two-tailed $t$-test, $t_{(99)} = 11.2$, $P < 0.001$, for the hand motor network; paired two-tailed $t$-test, $t_{(99)} = 21.9$, $P < 0.001$ for the language network), with Dice coefficients of 66.6% ± 10.2% for the hand motor network and 61.5% ± 9.1% (mean ± s.d.) for the language networks. Although the task data analyzed here reflect only a subset of possible tasks and range of data quality that could be explored, it is notable that the present iterative parcellation approach performed comparably and, in many individuals, better than traditional task-based analysis.

### Validation by electrical cortical stimulation

To further validate the results derived from the iterative parcellation approach, we used a clinical data set from eight surgical patients who performed a battery of motor tasks in MRI before surgery (data set IV). Resting-state data were also collected in six of the patients. Their hand and tongue sensorimotor regions were localized using electrical cortical stimulation (ECS), the current 'gold standard' for preoperative functional mapping. This data set provided an opportunity to evaluate the clinical applicability of the iterative parcellation technique. Parcellation was performed in each patient on the basis of the motor task fMRI data that were bandpass filtered (0.01– 0.08 Hz) and processed in the same way as in the 100 HCP subjects (data set II). The hand and tongue regions were also mapped using the traditional task-activation approach for comparison.

Sensorimotor regions identified by ECS were used as references (**Fig. 5a**). Motor and sensory regions identified by traditional task activation showed low consistency with the ECS maps (**Fig. 5b**). In contrast, the sensorimotor regions identified by iterative parcellation were more consistent with the ECS maps (**Fig. 5c**), suggesting that the iterative parcellation technique was valid and could serve as a prescreening method for ECS (**Supplementary Fig. 6**). In addition, a parcellation map of multiple functional networks with confidence values greater than a predetermined threshold (for example, an arbitrary threshold of 1.1) can provide a rough estimate of the ROIs for invasive cortical stimulation (**Fig. 5d**), potentially shortening the stimulation procedure.

To assess the potential of our parcellation technique in preoperative mapping, we statistically evaluated the sensitivity and specificity of the hand and tongue sensorimotor maps from the eight surgical patients in data set IV across different confidence thresholds. Sensitivity and specificity of the task fMRI were also computed by varying the $t$ thresholds of the task activation. In addition, we masked the task-activation maps using the pre-central and post-central gyri labels generated by FreeSurfer to improve specificity. This operation mimics the procedure of human experts, who usually disregard the noisy activation responses outside the ROIs. Receiver operating characteristic (ROC) curves were then plotted for the iterative parcellation algorithm (**Fig. 5e**), traditional task-activation mapping alone and task-activation masked with anatomical labels. The iterative parcellation technique significantly outperformed the other two task-based methods and showed a significantly larger area under the curve (AUC) ($P = 0.008$ and $P = 0.015$, Wilcoxon rank-sum test; AUC of iterative parcellation = 0.91, AUC of task fMRI = 0.76, AUC of task fMRI masked with anatomical labels = 0.78).

We then applied the iterative parcellation to the pure resting-state data in six patients from data set IV (**Fig. 5e**). The ROC curve was not significantly different from the original parcellation results based on the task fMRI data (AUC = 0.91 versus 0.89, $P = 0.22$, Wilcoxon rank-sum test). Finally, we examined whether using the iterative parcellation was truly advantageous over using the population-based atlas for each individual subject (**Fig. 5e** and **Supplementary Fig. 6**). The iterative parcellation technique significantly outperformed the population atlas (AUC = 0.91 versus 0.78, $P = 0.015$, Wilcoxon rank-sum test) in motor mapping.

## DISCUSSION

Here we present an approach for parcellating functional networks across the cerebral cortex in individuals on the basis of functional connectivity. Each brain had unique features. Parcellation networks were reproducible within subjects across multiple scans and could capture inter-individual differences in functional organization, including variability in brain lateralization. We found that this approach can be applied to various populations and extended to task fMRI data. Using invasive cortical stimulation as the gold standard, we evaluated the sensitivity and specificity of iterative functional parcellation in surgical patients and compared them to that of conventional task fMRI. Our results indicate that the individual cortical parcellation technique can correctly localize functional networks in individual subjects and has potential for use in clinical applications.

### Revealing individual variability in brain organization

Inter-individual variability in human brain organization has long been studied[39]. However, systematic *in vivo* research on the variability in the functional organization of the human brain, especially in the patterns of connectivity, has just begun. Variability in functional connectivity has been related to individual differences in human behavior and cognition, such as IQ, musical ability and reading ability[24]. Brain changes associated with neurological and psychiatric disorders are also reflected by variations in functional connectivity[40]. Recent explorations of resting-state functional connectivity in healthy humans have suggested that association regions (including

the language, executive control and attention networks) show particularly strong variability that may relate to individual differences in behavior[31,41]. Substantial inter-individual variability in functional organization calls for imaging techniques that can capture precisely the functional characteristics of each subject. To enable functional analyses at the individual-level, Carddock *et al.* parcellated rs-fMRI data into functionally and spatially coherent ROIs that tended to be equally sized[30]. Arslan *et al.* proposed a cortical parcellation method based on spectral graph theory and were able to obtain reliable results at the group level; however, inter-subject variability was underestimated and the method aimed to identify a group-wise parcellation that could represent each subject in the group[42]. Goulas *et al.* parcellated the lateral frontal cortex using a module detection algorithm and demonstrated inter-subject variability in these modules; however, intra-subject reliability was not evaluated at the same time[29]. Using a region-growing method, Blumensath *et al.* mapped functional networks in individual subjects with high reproducibility[28] and found that functional connectivity network boundaries might overlap with task activations. These important technical developments merit validation, especially that based on invasive measures. A precise parcellation technique with high sensitivity to individual variations will facilitate discovery of meaningful biomarkers for cognitive ability or disease states and provide greater statistical power for investigating behavioral or genetic associations.

### Implications for clinical intervention

An individual-level functional atlas has strong implications for clinical practice, especially for surgical planning and brain stimulation that depend on precise functional localization. Current preoperative mapping with task-based fMRI is hampered by poor SNR, limited test-retest reliability and limited overlap with analogous maps derived from invasive cortical stimulation[43,44], raising questions about its clinical utility. For example, a meta-analysis of 63 published studies found that task fMRI has only moderate (~50%) within-subject test-retest reproducibility[38]. In the present study, limited reproducibility was also observed between the two runs of task fMRI data in the HCP subjects. This was due in part to the limited acquisition length of the task runs and variability in data quality, but iterative parcellation based on the same amount of data was significantly more reliable. In addition, the iterative parcellation can be applied directly to bandpass-filtered task fMRI data and produce functional maps comparable to maps based on pure resting-state data (**Figs. 3d** and **5e**). In a small group of surgical patients, we found that sensorimotor networks could be localized with higher accuracy by the iterative parcellation than by conventional task fMRI.

The advantage of the iterative parcellation over conventional task fMRI may be explained by the different amount of variance in the BOLD signal they use for mapping. Task-evoked activity accounts for a small percentage of the total variance in fMRI signal and therefore provides less stability, as the practical limits of scanning burden constrain the amount of task data that can be acquired, especially in patient populations. Variance used in task-activation mapping can be estimated on the basis of the variance explained by the hemodynamic task model. In the eight surgical patients reported in the present study (data set IV), task-related activity in the motor regions of interest defined by ECS accounted for only 32.5% of the total variance in the functional MRI signal. Prior work has shown that coherent spontaneous activity does not cease during task paradigms[45]. Our parcellation approach utilizes spontaneous activity for mapping, which may account for the major portion of the variance in task fMRI BOLD signal[45].

To render this parcellation strategy useful in mapping the language and memory networks in patients, further optimization and validation are necessary. Nevertheless, our preliminary observations indicate that parcellation can reliably identify a strongly left-lateralized network overlapping with the regions activated by a language task and a right-lateralized network that is located in traditional ventral attention regions. Additionally, lateralization of these networks may relate to handedness. These observations suggest that this iterative individually tailored parcellation captures a large portion of the individual variability present in the organization of cerebral networks.

### Improving cross-subject alignment for group analysis

Establishing the functional correspondence between subjects is a prerequisite for group-level functional imaging analyses. Although the association between brain anatomy and function is not fully understood and can vary across individuals, most fMRI processing tools align individual subjects to a common template on the basis of anatomical features such as global morphology or landmarks identified by structural MRI[46,47]. Functional networks are likely to be misaligned if they are not tightly linked to the macroscopic anatomy. For example, aligning subjects for the investigation of language function can be particularly challenging, because the distribution of the language network is highly variable and can even be located in different hemispheres in different individuals. Substantial inter-subject variability in functional regions was found even after careful alignment of the data on the basis of curvature, which largely removed macro-anatomical variability[19]. Recent studies have attempted to align subjects on the basis of functional characteristics. By incorporating the inter-subject signal correlations into a cortical registration algorithm, Subuncu *et al.* brought functionally similar regions into correspondence during a movie-watching task[48]. However, this strategy relies on consistent task activations across subjects. Robinson *et al.* developed a method capable of aligning subjects using a wide variety of characteristics, including structure and function[49]. The authors demonstrated strong increases, compared to curvature-based registration, in the cluster mass of task activations when subjects were aligned on the basis of resting-state functional connectivity. The development of functional network parcellation using resting-state connectivity[10,11], especially parcellation at the individual level[14,27], may offer a complementary connectivity-based functional localizer for group-level analyses. A parcellation like the one we describe here can provide a set of functional landmarks for cross-subject registration and lead to new strategies for brain image alignment.

### Limitations and future directions

The present study has several technical limitations. First, the number of networks was selected according to specific technical criteria instead of biological considerations[10]. The fixed number of networks may not be appropriate for all individuals, especially for those who have experienced functional reorganization due to disease. In some patients, certain networks may be completely absent. For example, one subject in our study showed substantial reorganization of the tongue motor area owing to encephalomalacia (subject 5, **Supplementary Fig. 6**). This change in functional organization led to misalignment of the hand motor networks in the parcellation, where the hand network spread to lower portions of the post-central gyrus. Thus, additional improvement and validation of this iterative functional parcellation method are required before it can be applied to patients with distorted anatomy. For example, in patients with localized lesions (limited to one hemisphere), the iterative functional parcellation could be performed in the healthy hemisphere without distortion, as well as in

the cerebellum, if no lesions are observed. The functional properties in the affected hemisphere could then be estimated on the basis of its functional connectivity to the healthy cerebral hemisphere or the unaffected cerebellum.

Second, we parcellated the cortex into a relatively small number of networks, which can reduce the sensitivity to subtle changes in functional networks, such as those due to learning or other experiences. Future development of the parcellation technology should aim at mapping functional networks with finer spatial resolution and determining the number of networks more flexibly in different subjects. A possible strategy is to initiate the iterative parcellation from a population-based atlas with a large number of networks and gradually adjust the number of networks by merging networks with similar time courses (for example, $r > 0.5$). Once a merger occurs, the iterative parcellation can be restarted with the reduced number of networks. This strategy flexibly adjusts the number of networks on the basis of an individual's data and can accommodate the need for identifying small networks. Iterative parcellation with this flexible strategy can also achieve high reproducibility (**Supplementary Fig. 7**). Alternative strategies, such as estimation of regions on the basis of local transitions in connectivity properties, are also possible[13–15].

Finally, functional maps derived from fMRI data can be influenced by various confounding factors. For example, spatial specificity of the functional connectivity maps can be influenced by the signal in macroscopic veins, and signal correlations can be overstated within or between highly vascularized regions[50]. Thus, inter-subject variability observed in functional connectivity patterns can also be confounded by variations in vascular anatomy. Although it is difficult to quantify the contribution of vascular variation, the high inter-subject variability in functional connectivity in the association cortex (especially in hemispheric lateralization) is unlikely to be dominated by vascular variations, but the contributions of vascular anatomy to the topographical maps studied here will be critical.

## METHODS

Methods and any associated references are available in the online version of the paper.

*Note: Any Supplementary Information and Source Data files are available in the online version of the paper.*

### ACKNOWLEDGMENTS

The authors thank X. Peng and M. Li for technical assistance. Data set II was provided by the Human Connectome Project, WU-Minn Consortium (principal investigators, D. Van Essen and K. Ugurbil; 1U54MH091657) funded by the 16 NIH Institutes and Centers that support the NIH Blueprint for Neuroscience Research; and by the McDonnell Center for Systems Neuroscience at Washington University. Data set III was provided by the Brain Genomics Superstruct Project of Harvard University and the Massachusetts General Hospital (principal investigators, R.L.B., J. Roffman and J. Smoller), with support from the Center for Brain Science Neuroinformatics Research group, the Athinoula A. Martinos Center for Biomedical Imaging, and the Center for Human Genetic Research. Twenty investigators at Harvard and MGH contributed data to the overall project. This work was supported by NIH grants K25NS069805 (H.L.), R01NS091604 (H.L.), P50MH106435 (R.L.B. and H.L.), K01MH099232 (A.J.H.), R01HD067312 (G.L.), P41EB015902 (G.L.), OeNB Nr. 15929 (G.L.), Medical Imaging Cluster of the Medical University of Vienna (G.L.), National Basic Research Program of China Grant 2011CB504100 (X.W.), National Science Foundation of China Grant 61473169 (B.H.) and National Program on Key Basic Research Projects of China Grant 2011CB933204 (B.H.).

### AUTHOR CONTRIBUTIONS

D.W., R.L.B. and H.L. conceived the study; D.W. and H.L. designed the algorithm and performed the analyses in healthy subjects with support from S.S., G.L. and R.P.; H.L., B.H., M.D.F. and T.Q. designed and performed the analyses in patients; D.J.H., A.J.H., K.L., J.T.B., S.M.S., K.W. and X.W. provided support and guidance with data interpretation. H.L., D.W. and R.L.B. wrote the manuscript with contribution from M.D.F. and D.J.H. All authors commented on the manuscript.

### COMPETING FINANCIAL INTERESTS

The authors declare competing financial interests: details are available in the online version of the paper.



1. Brodmann, K. *Brodmann's: Localisation in the Cerebral Cortex* 3rd edn. (Springer, 2006).
2. Kaas, J.H. The organization of neocortex in mammals: implications for theories of brain function. *Annu. Rev. Psychol.* **38**, 129–151 (1987).
3. Toga, A.W., Thompson, P.M., Mori, S., Amunts, K. & Zilles, K. Towards multimodal atlases of the human brain. *Nat. Rev. Neurosci.* **7**, 952–966 (2006).
4. Zilles, K. & Amunts, K. Centenary of Brodmann's map—conception and fate. *Nat. Rev. Neurosci.* **11**, 139–145 (2010).
5. Amunts, K. *et al.* Broca's region revisited: cytoarchitecture and intersubject variability. *J. Comp. Neurol.* **412**, 319–341 (1999).
6. Goldman-Rakic, P.S. Topography of cognition: parallel distributed networks in primate association cortex. *Annu. Rev. Neurosci.* **11**, 137–156 (1988).
7. Felleman, D.J. & Van Essen, D.C. Distributed hierarchical processing in the primate cerebral cortex. *Cereb. Cortex.* **1**, 1–47 (1991).
8. Biswal, B., Yetkin, F.Z., Haughton, V.M. & Hyde, J.S. Functional connectivity in the motor cortex of resting human brain using echo-planar MRI. *Magn. Reson. Med.* **34**, 537–541 (1995).
9. Fox, M.D. & Raichle, M.E. Spontaneous fluctuations in brain activity observed with functional magnetic resonance imaging. *Nat. Rev. Neurosci.* **8**, 700–711 (2007).
10. Yeo, B.T. *et al.* The organization of the human cerebral cortex estimated by intrinsic functional connectivity. *J. Neurophysiol.* **106**, 1125–1165 (2011).
11. Power, J.D. *et al.* Functional network organization of the human brain. *Neuron* **72**, 665–678 (2011).
12. Shen, X., Tokoglu, F., Papademetris, X. & Constable, R.T. Groupwise whole-brain parcellation from resting-state fMRI data for network node identification. *Neuroimage* **82**, 403–415 (2013).
13. Gordon, E.M. *et al.* Generation and evaluation of a cortical area parcellation from resting-state correlations. *Cereb. Cortex* doi:10.1093/cercor/bhu239 (2014).
14. Wig, G.S. *et al.* Parcellating an individual subject's cortical and subcortical brain structures using snowball sampling of resting-state correlations. *Cereb. Cortex* **24**, 2036–2054 (2013).
15. Wig, G.S., Laumann, T.O. & Petersen, S.E. An approach for parcellating human cortical areas using resting-state correlations. *Neuroimage* **93**, 276–291 (2014).
16. Laumann, T.O. *et al.* Functional system and areal organization of a highly sampled individual human brain. *Neuron* **87**, 657–670 (2015).
17. Penfield, W. & Jasper, H.H. *Epilepsy and the Functional Anatomy of the Human Brain* (Little, 1954).
18. Ojemann, G., Ojemann, J., Lettich, E. & Berger, M. Cortical language localization in left, dominant hemisphere. An electrical stimulation mapping investigation in 117 patients. *J. Neurosurg.* **71**, 316–326 (1989).
19. Frost, M.A. & Goebel, R. Measuring structural-functional correspondence: spatial variability of specialised brain regions after macro-anatomical alignment. *Neuroimage* **59**, 1369–1381 (2012).
20. Binder, J.R. *et al.* Human brain language areas identified by functional magnetic resonance imaging. *J. Neurosci.* **17**, 353–362 (1997).
21. Fox, M.D., Liu, H. & Pascual-Leone, A. Identification of reproducible individualized targets for treatment of depression with TMS based on intrinsic connectivity. *Neuroimage* **66**, 151–160 (2013).
22. Fox, M.D. *et al.* Resting state networks link invasive and noninvasive brain stimulation across diverse psychiatric and neurological diseases. *Proc. Natl. Acad. Sci. USA* **111**, E4367–E4375 (2014).
23. Binder, J.R. Functional MRI is a valid noninvasive alternative to Wada testing. *Epilepsy Behav.* **20**, 214–222 (2011).
24. Wang, D. & Liu, H. Functional connectivity architecture of the human brain: not all the same. *Neuroscientist* **20**, 432–438 (2014).
25. Fedorenko, E., Hsieh, P.J., Nieto-Castanon, A., Whitfield-Gabrieli, S. & Kanwisher, N. New method for fMRI investigations of language: defining ROIs functionally in individual subjects. *J. Neurophysiol.* **104**, 1177–1194 (2010).
26. Sohn, W.S. *et al.* Influence of ROI selection on resting state functional connectivity: an individualized approach for resting state fMRI analysis *Front. Neurosci.* **9**, 280 (2015).
27. Hacker, C.D. *et al.* Resting state network estimation in individual subjects. *Neuroimage* **82**, 616–633 (2013).
28. Blumensath, T. *et al.* Spatially constrained hierarchical parcellation of the brain with resting-state fMRI. *Neuroimage* **76**, 313–324 (2013).
29. Goulas, A., Uylings, H.B. & Stiers, P. Unravelling the intrinsic functional organization of the human lateral frontal cortex: a parcellation scheme based on resting state fMRI. *J. Neurosci.* **32**, 10238–10252 (2012).
30. Craddock, R.C., James, G.A., Holtzheimer, P.E. III, Hu, X.P. & Mayberg, H.S. A whole brain fMRI atlas generated via spatially constrained spectral clustering. *Hum. Brain Mapp.* **33**, 1914–1928 (2012).

31. Mueller, S. *et al.* Individual variability in functional connectivity architecture of the human brain. *Neuron* **77**, 586–595 (2013).
32. Poldrack, R.A. & Gorgolewski, K.J. Making big data open: data sharing in neuroimaging. *Nat. Neurosci.* **17**, 1510–1517 (2014).
33. Krienen, F.M., Yeo, B.T. & Buckner, R.L. Reconfigurable task-dependent functional coupling modes cluster around a core functional architecture. *Phil. Trans. R. Soc. Lond. B* **369**, 20130526 (2014).
34. Cole, M.W., Bassett, D.S., Power, J.D., Braver, T.S. & Petersen, S.E. Intrinsic and task-evoked network architectures of the human brain. *Neuron* **83**, 238–251 (2014).
35. Wang, D., Buckner, R.L. & Liu, H. Functional specialization in the human brain estimated by intrinsic hemispheric interaction. *J. Neurosci.* **34**, 12341–12352 (2014).
36. Corbetta, M. & Shulman, G.L. Control of goal-directed and stimulus-driven attention in the brain. *Nat. Rev. Neurosci.* **3**, 201–215 (2002).
37. Barch, D.M. *et al.* Function in the human connectome: task-fMRI and individual differences in behavior. *Neuroimage* **80**, 169–189 (2013).
38. Bennett, C.M. & Miller, M.B. How reliable are the results from functional magnetic resonance imaging? *Ann. NY Acad. Sci.* **1191**, 133–155 (2010).
39. Swaab, D.F. & Hofman, M.A. Sexual differentiation of the human brain. A historical perspective. *Prog. Brain Res.* **61**, 361–374 (1984).
40. Fox, M.D. & Greicius, M. Clinical applications of resting state functional connectivity. *Front. Syst. Neurosci.* **4**, 19 (2010).
41. Gao, W. *et al.* Intersubject variability of and genetic effects on the brain's functional connectivity during infancy. *J. Neurosci.* **34**, 11288–11296 (2014).
42. Arslan, S., Parisot, S. & Rueckert, D. Joint spectral decomposition for the parcellation of the human cerebral cortex using resting-state fMRI. *Inf. Process. Med. Imaging* **24**, 85–97 (2015).
43. Giussani, C. *et al.* Is preoperative functional magnetic resonance imaging reliable for language areas mapping in brain tumor surgery? Review of language functional magnetic resonance imaging and direct cortical stimulation correlation studies. *Neurosurgery* **66**, 113–120 (2010).
44. Binder, J.R., Swanson, S.J., Hammeke, T.A. & Sabsevitz, D.S. A comparison of five fMRI protocols for mapping speech comprehension systems. *Epilepsia* **49**, 1980–1997 (2008).
45. Fox, M.D., Snyder, A.Z., Zacks, J.M. & Raichle, M.E. Coherent spontaneous activity accounts for trial-to-trial variability in human evoked brain responses. *Nat. Neurosci.* **9**, 23–25 (2006).
46. Fischl, B., Sereno, M.I. & Dale, A.M. Cortical surface-based analysis. II: Inflation, flattening, and a surface-based coordinate system. *Neuroimage* **9**, 195–207 (1999).
47. Woolrich, M.W. *et al.* Bayesian analysis of neuroimaging data in FSL. *Neuroimage* **45**, S173–S186 (2009).
48. Sabuncu, M.R. *et al.* Function-based intersubject alignment of human cortical anatomy. *Cereb. Cortex* **20**, 130–140 (2010).
49. Robinson, E.C. *et al.* MSM: a new flexible framework for Multimodal Surface Matching. *Neuroimage* **100**, 414–426 (2014).
50. Curtis, A.T., Hutchison, R.M. & Menon, R.S. Phase based venous suppression in resting-state BOLD GE-fMRI. *Neuroimage* **100**, 51–59 (2014).

## ONLINE METHODS

**Participants and data collection.** Four fMRI data sets obtained with different imaging parameters were employed in the current study.

*Data set I.* The first data set consists of 25 healthy subjects (age 51.8 ± 6.99 (mean ± s.d.), nine female, two left handed) enrolled as a control data set in a longitudinal fMRI study on stroke recovery. Participants were screened to exclude individuals with a history of neurologic or psychiatric conditions, as well as those using psychoactive medications. Each subject underwent five scanning sessions within 6 months (7, 14, 30, 90 and 180 d from enrollment). All participants performed two or three resting-state runs per session (6 m 12 s per run) to estimate intrinsic functional connectivity. After quality control, 23 subjects who had at least two good runs (tSNR > 100) in each session were included in this study (mean = 2.02 runs). This data set has been previously reported[31]. MRI data were acquired on a 3 Tesla Siemens TimTrio system (Erlangen, Germany) using the 12-channel phased-array coil supplied by the vendor. Structural images were acquired using a sagittal MP-RAGE three-dimensional T1-weighted sequence (TR = 1,600 ms; TE = 2.15 ms; flip angle = 9°; 1.0 mm isotropic voxels; FOV = 256 × 256). Functional data were obtained using a gradient echo-planar pulse sequence (TR = 3,000 ms; TE = 30 ms; flip angle = 90°; 3 mm isotropic voxels, transverse orientation, 47 slices fully covering cerebral cortex and cerebellum). Subjects were instructed to stay awake and keep their eyes open. Participants provided written informed consent in accordance with guidelines set by the institutional review boards of Xuanwu Hospital.

*Data set II.* The second data set included 100 young healthy volunteers (the 'Unrelated 100', 54 female, age 22–35 years, except one subject, who was more than 36 years old) made publicly available by the Human Connectome Project supported by the WU-Minn Consortium[51]. Written informed consent was obtained from each participant in accordance with guidelines and regulations approved by the local institutional review board at Washington University in St. Louis (IRB #201204036). For each participant, two resting-state fMRI sessions (each session consisted of one run with left-to-right direction phase encoding and one run with right-to-left direction) and seven task fMRI sessions (each session consisted of one run with left-to-right direction phase encoding and one run with right-to-left direction) were obtained. The tasks included working memory (5 m 1 s per run), gambling (3 m 12 s per run), motor (3 m 34 s per run), language (3 m 57 s per run), social cognition (3 m 27 s per run), relational processing (2 m 56 s per run) and emotional processing (2 m 16 s per run). A complete description of the data set has been published[51,52].

All HCP subjects were scanned on a customized Siemens 3T Connectome Skyra scanner. Structural images were acquired using the 3D MPRAGE T1-weighted sequence with 0.7 mm isotropic resolution (FOV = 224 mm, matrix = 320, 256 sagittal slices in a single slab, TR = 2,400 ms, TE = 2.14 ms, TI = 1,000 ms, flip angle = 8°). The scan parameters of the rs-fMRI data were as follows: TR = 720 ms; TE = 33.1 ms; flip angle = 52°; FOV = 208 × 180 mm; slice thickness = 2.0 mm; 72 slices; 2 mm isotropic voxels, multiband factor = 8; echo spacing = 0.58 ms; bandwidth (BW) = 2,290 Hz/px; time points = 1,200. The task acquisitions were identical to the resting-state fMRI acquisitions in order to provide maximal compatibility between task and resting data.

*Data set III.* The third data set included data of 52 left-handed and 52 matched right-handed subjects (28 female in each group, 18–25 years) that were acquired as part of the Brain Genomics Superstruct Project[53]. All participants provided written informed consent in accordance with guidelines set by the Institutional Review Boards of Harvard University or Partners Healthcare. Each subject performed two resting-state (eyes open) runs in MRI scanner (6 m 12 s per run). All data were collected on matched 3T Tim Trio scanners (Siemens, Erlangen, Germany) using a 12-channel phased-array head coil. Images were acquired using the gradient-echo echo-planar pulse sequence (TR = 3,000 ms, TE = 30 ms, flip angle = 85°, 3 × 3 × 3 mm voxels, FOV = 216 and 47 slices collected with interleaved acquisition with no gap between slices). Whole brain coverage including the entire cerebellum was achieved with slices aligned to the anterior commissure-posterior commissure plane using an automated alignment procedure, ensuring consistency among subjects[54]. Structural data included a high-resolution multi-echo T1-weighted magnetization-prepared gradient-echo image (TR = 2,200 ms, TI = 1,100 ms, TE = 1.54 ms for image 1 to 7.01 ms for image 4, flip angle = 7°, 1.2 × 1.2 × 1.2 mm and FOV = 230). Subjects were instructed to stay awake, keep their eyes open, and minimize head movement; no other task instruction was provided. The handedness of each subject was assessed via the Edinburgh handedness inventory[55]. The demographic information of the 52 pairs of subjects and the matching criteria are listed in **Supplementary Table 1**.

*Data set IV.* The fourth data set included eight surgical candidates (age 19.5 ± 5.0; five female; one left handed) with intractable epilepsy. This was a subset of patients from a published study of cortical mapping using gamma activity recorded from subdural electrode grids[56]. The experiment included a preoperative fMRI scan, surgical implantation of subdural electrode grids and direct electrical cortical stimulation (ECS) using these grids. No seizures were observed 1 h before or after the fMRI or ECS in all patients. The locations of the electrodes and how long they would stay implanted were determined solely by clinical criteria. Written consent was obtained from each patient or their guardians, and the experiments were approved by the Ethics Committees of the Second Affiliated Hospital of Tsinghua University. MRI data were collected on a Philips Achieva 3.0 Tesla TX whole body MR scanner using an 8-channel SENSE head coil. Structural images were acquired using a sagittal magnetization-prepared rapid gradient echo T1-weighted sequence (TR = 8.1 ms, TE = 3.7 ms, TI = 1,000 ms, flip angle = 8°, FOV = 230 mm × 230 mm, matrix size = 230 × 230, slices = 180, voxel size = 1 × 1 × 1 mm). Functional data were collected using an echo planar imaging sequence (TR = 3,000 ms, TE = 30 ms, flip angle = 90°, FOV = 192 mm × 192 mm, matrix size = 64 × 64, slices = 47, voxel size = 3 × 3 × 3 mm).

Two types of functional runs were collected from the epilepsy patients: task activation runs (all eight subjects) and resting state runs (six of eight subjects). All eight subjects performed five motor task activation runs. Each run consisted of one type of self-paced movement (left hand, right hand, left foot, right foot, or tongue) consistent with standard preoperative mapping paradigms. Each run was 144 s long and consisted of six 12-s task blocks interleaved with six 12-s rest intervals. Patients performed motor tasks according to the instructions presented on the computer screen using the Psychophysics Toolbox in MATLAB (MathWorks, Inc.). Six subjects also underwent two resting-state runs (360 s each run), during which they were asked to fixate on a crosshair in the center of the screen. These pure resting state runs were collected for comparison purposes with the maps created based on the task runs.

After an adequate number of seizures had been recorded, bedside ECS mapping was performed to identify the sensorimotor cortices[56]. Using an Ojemann Cortical Stimulator (Integra Life-Sciences), trains of 60-Hz biphasic pulses lasting 2–5 s were delivered to selected pairs of electrodes. The current intensity of the stimulation started at 2 mA and was gradually increased until patients showed or reported symptoms related to the sensorimotor cortex or the stimulus strength reached 15 mA. Each stimulation involved a pair of electrodes; thus, both electrodes were considered positive when a hand or tongue movement or sensory was produced.

**Data processing.** *Data set I.* Resting-state fMRI data of the 23 subjects in this longitudinal data set were processed using the procedures described[8,10,57]. The following steps were performed: (i) slice timing correction (SPM2; Wellcome Department of Cognitive Neurology, London, UK), (ii) rigid body correction for head motion with the FSL package[58,59], (iii) normalization for global mean signal intensity across runs, and (iv) bandpass temporal filtering (0.01– 0.08 Hz), head-motion regression, whole-brain signal regression, and ventricular and white-matter signal regression. The BOLD frames were not censored based on head motion but all runs included in the present study showed temporal SNR > 100.

Structural data were processed using FreeSurfer version 4.5.0. Surface mesh representations of the cortex from each individual subject's structural images were reconstructed and registered to a common spherical coordinate system[46]. The structural and functional images were aligned using boundary-based registration[60] within the FsFast software package (http://surfer.nmr.mgh.harvard.edu/fswiki/FsFast). The preprocessed resting-state BOLD fMRI data were then aligned to the common spherical coordinate system via sampling from the middle of the cortical ribbon in a single interpolation step[10]. FMRI data of each individual were first registered to the FreeSurfer template that consisted of 40,962 vertices in each hemisphere. A 6-mm full-width half-maximum (FWHM) smoothing kernel was then applied to the fMRI data in the surface space. The smoothed data were then down-sampled to a mesh of 2,562 vertices in each hemisphere using the mri_surf2surf function in FreeSurfer software.

*Data set II.* The 'minimally processed' fMRI data of the HCP subjects were used, which had been preprocessed in the HCP pipeline using FSL (FMRIB Software Library), FreeSurfer, and the Connectome Workbench software[37,61–63].

The preprocessed data were projected to the FreeSurfer template with a mesh of 40,962 vertices in each hemisphere. The following steps were then performed: (i) demeaning and detrending across each run, (ii) bandpass filtering (0.01–0.08Hz), (iii) head-motion regression and whole-brain signal regression and (iv) smoothing with a 6-mm FWHM smoothing kernel in the surface space. The data were then down-sampled to a mesh of 2,562 vertices in each hemisphere using the mri_surf2surf function provided by FreeSurfer. For connectivity analyses, the task fMRI data were processed in the same way as the resting-state data. To map the brain regions activated by the seven tasks, fixed-effects analyses were performed using FEAT[37,61].

*Data set III.* Resting-state fMRI data of the 52 pairs of left-handed and right-handed subjects were preprocessed identically to the first data set.

*Data set IV.* For parcellation analysis, bandpass filtered task fMRI and pure resting-state fMRI data of the surgical patients were preprocessed identically to the first data set. Conventional task-evoked activation maps in this data set were estimated using the general linear model. Regressors of no interest included motion correction parameters and low frequency drift. The task-induced BOLD response was modeled by convolving the hemodynamic response function with the experimental design. Intracranial electrodes were registered to the cortical surface using in-house software[56] to enable the comparison between the ECS maps and the functional parcellation. A post-implantation CT scan was obtained within 24–48 h after the implant surgery for localization of the electrodes. The post-implantation CT images were registered to T1-weighted MRI images using a mutual-information-based linear transform[56]. Owing to postoperative edema, electrodes extracted from the post-implantation CT images may appear off the surface reconstructed from the presurgical MRI. Our in-house tool allows us to manually adjust the locations of electrodes according to the 3D shape of the cortical surface. MRI surface vertices within a 6 mm radius of the positive electrodes were defined as positive. This resulted in an ECS map on the surface that can be directly compared to the map obtained from the functional parcellation.

**Population-based functional atlas.** A functional network atlas was estimated based on 1,000 healthy subjects[10] and projected onto the individual subject's cortical surface using the FreeSurfer software. The original atlas included 17 networks where hand sensorimotor areas were not separated from other areas. Given the common need to map hand areas in surgical patients, we identified the hand sensorimotor areas from this atlas on the basis of activations in a hand motor task[64]. As a result, this population atlas consisted of 18 networks and would serve as the initial guess of the functional network organization in an individual subject's brain.

**Evaluating test-retest reliability and inter-subject variability of the maps derived from the iterative parcellation.** Intra-subject test-retest reliability of the parcellation results was computed using the Dice coefficient after projecting the parcellation results back to each subject's cortical surface. This can be simply computed as the percentage of vertices that were assigned to the same network in two sessions. To assess the reliability of the parcellation technique at the group level, Dice coefficients were then averaged across all subjects. Inter-subject variability was computed on the FreeSurfer surface template (2,562 vertices in each hemisphere) based on the Dice coefficient between any pair of subjects and then averaged across all pairs.

**Comparing the task fMRI and iterative parcellation with the ECS findings.** For the patient data set (data set IV), the results of different mapping modalities were projected to each patient's cortical surface for comparison with the ECS findings. Taking the ECS findings as references, the sensitivity and specificity of the activation map and the network parcellation were quantified. Sensitivity was computed by dividing the number of true positives (fMRI positive vertices that were also positive in the ECS maps) by the number of true positives plus false negatives (i.e., total vertices positive in the ECS maps). The specificity was computed by the number of true negatives (fMRI negative vertices that were also negative in the ECS maps) divided by the number of true negatives plus false positives (i.e. total vertices negative in the ECS maps). ROC curves were obtained by calculating the sensitivity and specificity across a wide range of different thresholds. The area under the curve was computed for each subject and compared across methods using a Wilcoxon paired nonparametric test.

**Estimating functional lateralization.** Lateralization was computed for each network derived from the iterative parcellation. Vertices that belonged to a specific network were separated into left-hemisphere and right-hemisphere portions. A lateralization index was then computed based on the following equation:

$$LI = (V_L - V_R)/(V_L + V_R) \quad (1)$$

Where $V_L$ is the number of vertices in the left hemisphere, $V_R$ is the number of vertices in the right hemisphere.

**Visualization and statistics.** The iterative parcellation was performed on the FreeSurfer fsaverage4 template and the resulting network labels were upsampled to each individual subject's own cortical surface using the mri_surf2surf function. The labels were then merged into a single 'annotation' file using the write_annotation function provided by FreeSurfer. The parcellation results were visualized in each individual's cortical surface using FreeSurfer.

No statistical methods were used to pre-determine sample sizes but our sample sizes are larger than or similar to those reported in previous publications[31,37,65,66]. Within each data set, no randomization or blinding was employed to separate subjects into different groups. Two-tailed *t*-test was used for all comparisons in this study except for the experiment shown in **Figure 5**, which used Wilcoxon rank-sum test. For the *t*-tests, data distribution was assumed to be normal, but this was not formally tested.

**Code availability.** The code of the iterative parcellation algorithm is available upon request.

A **Supplementary Methods Checklist** is available.


51. Van Essen, D.C. *et al.* The WU-Minn Human Connectome Project: an overview. *Neuroimage* **80**, 62–79 (2013).
52. Van Essen, D.C. *et al.* The Human Connectome Project: a data acquisition perspective. *Neuroimage* **62**, 2222–2231 (2012).
53. Holmes, A.J. *et al.* Brain Genomics Superstruct Project initial data release with structural, functional, and behavioral measures. *Sci. Data.* **2**, 150031 (2015).
54. van der Kouwe, A.J., Benner, T., Salat, D.H. & Fischl, B. Brain morphometry with multiecho MPRAGE. *Neuroimage* **40**, 559–569 (2008).
55. Oldfield, R.C. The assessment and analysis of handedness: the Edinburgh inventory. *Neuropsychologia* **9**, 97–113 (1971).
56. Qian, T. *et al.* Fast presurgical functional mapping using task-related intracranial high gamma activity. *J. Neurosurg.* **119**, 26–36 (2013).
57. Fox, M.D. *et al.* The human brain is intrinsically organized into dynamic, anticorrelated functional networks. *Proc. Natl. Acad. Sci. USA* **102**, 9673–9678 (2005).
58. Jenkinson, M., Bannister, P., Brady, M. & Smith, S. Improved optimization for the robust and accurate linear registration and motion correction of brain images. *Neuroimage* **17**, 825–841 (2002).
59. Smith, S.M. *et al.* Advances in functional and structural MR image analysis and implementation as FSL. *Neuroimage* **23** (Suppl. 1), S208–S219 (2004).
60. Greve, D.N. & Fischl, B. Accurate and robust brain image alignment using boundary-based registration. *Neuroimage* **48**, 63–72 (2009).
61. Woolrich, M.W., Ripley, B.D., Brady, M. & Smith, S.M. Temporal autocorrelation in univariate linear modeling of FMRI data. *Neuroimage* **14**, 1370–1386 (2001).
62. Glasser, M.F. *et al.* The minimal preprocessing pipelines for the Human Connectome Project. *Neuroimage* **80**, 105–124 (2013).
63. Marcus, D.S. *et al.* Human Connectome Project informatics: quality control, database services, and data visualization. *Neuroimage* **80**, 202–219 (2013).
64. Buckner, R.L., Krienen, F.M., Castellanos, A., Diaz, J.C. & Yeo, B.T. The organization of the human cerebellum estimated by intrinsic functional connectivity. *J. Neurophysiol.* **106**, 2322–2345 (2011).
65. Wang, D., Buckner, R.L. & Liu, H. Cerebellar asymmetry and its relation to cerebral asymmetry estimated by intrinsic functional connectivity. *J. Neurophysiol.* **109**, 46–57 (2013).
66. Fox, M.D. *et al.* Combining task-evoked and spontaneous activity to improve pre-operative brain mapping with fMRI. *Neuroimage* **124**, 714–723 (2015).